

Leukotriene B₄ promotes neovascularization and macrophage recruitment in murine wet-type AMD models

Fumiyuki Sasaki,¹ Tomoaki Koga,¹ Mai Ohba,¹ Kazuko Saeki,¹ Toshiaki Okuno,¹ Keijiro Ishikawa,² Takahito Nakama,² Shintaro Nakao,² Shigeo Yoshida,² Tatsuro Ishibashi,² Hamid Ahmadi,³ Mozhgan Rezaei Kanavi,⁴ Ali Hafezi-Moghadam,⁵ Josef M. Penninger,⁶ Koh-Hei Sonoda,² and Takehiko Yokomizo¹

¹Department of Biochemistry, Juntendo University School of Medicine, Tokyo, Japan. ²Department of Ophthalmology, Graduate School of Medical Sciences, Kyushu University, Fukuoka, Japan. ³Ophthalmic Research Center, Shahid Beheshti University of Medical Sciences, Tehran, Iran. ⁴Ocular Tissue Engineering Research Center, Shahid Beheshti University of Medical Sciences, Tehran, Iran. ⁵Molecular Biomarkers Nano-Imaging Laboratory, Brigham & Women's Hospital, and Department of Radiology, Harvard Medical School, Boston, Massachusetts, USA. ⁶Institute of Molecular Biotechnology of the Austrian Academy of Sciences (IMBA), Vienna, Austria.

Age-related macular degeneration (AMD), a progressive chronic disease of the central retina, is associated with aging and is a leading cause of blindness worldwide. Here, we demonstrate that leukotriene B₄ (LTB₄) receptor 1 (BLT1) promotes laser-induced choroidal neovascularization (CNV) in a mouse model for wet-type AMD. CNV was significantly less in BLT1-deficient (BLT1-KO) mice compared with BLT1-WT controls. Expression of several proangiogenic and profibrotic factors was lower in BLT1-KO eyes than in BLT1-WT eyes. LTB₄ production in the eyes was substantially increased in the early phase after laser injury. BLT1 was highly expressed in M2 macrophages in vitro and in vivo, and ocular BLT1⁺ M2 macrophages were increased in the aged eyes after laser injury. Furthermore, M2 macrophages were rapidly attracted by LTB₄ and subsequently produced VEGF-A—through BLT1-mediated signaling. Consequently, intravitreal injection of M2 macrophages augmented CNV formation, which was attenuated by BLT1 deficiency. Thus, laser-induced injury to the retina triggered LTB₄ production and attracted M2 macrophages via BLT1, leading to development of CNV. A selective BLT1 antagonist (CP105696) and 3 LTB₄ inhibitors (zileuton, MK-886, and bestatin) reduced CNV in a dose-dependent manner. CP105696 also inhibited the accumulation of BLT1⁺ M2 macrophages in the laser-injured eyes of aged mice. Together, these results indicate that the LTB₄-BLT1 axis is a potentially novel therapeutic target for CNV of wet-type AMD.

Introduction

Age-related macular degeneration (AMD) is a chronic disease of the eye that is a leading cause of irreversible blindness in people over 50 years of age. AMD, which affects nearly 40 million individuals worldwide (1), is caused by deterioration of the retina, including the macula, which contains neuronal cells, photoreceptors, and retinal pigment epithelium (RPE) cells. AMD is classified as either wet type (also called neovascular or exudative) or dry type (also called geographic atrophy). Wet AMD is characterized by degeneration of the macula, accompanied by fluid leakage from choroidal neovessels that have invaded the retina. The lesion is infiltrated by immune cells such as macrophages, DC, microglial cells, and T cells (e.g., NKT and $\gamma\delta$ T cells) (2–4). The main treatments for wet AMD are agents that inhibit VEGF; however, such agents frequently require repeated intravitreal injection (IVI), which can cause infectious endophthalmitis, intraocular inflammation, and ocular hemorrhage (5).

Leukotriene B₄ receptor 1 (BLT1) is a G protein-coupled receptor (6) for a chemotactic eicosanoid, Leukotriene B₄ (LTB₄) (7, 8), which is generated from arachidonic acid by 5-lipoxygenase (5-LO), 5-lipoxygenase-activating protein (FLAP), and LTA₄ hydrolase (LTA₄H) (9) (Supplemental Figure 1; supplemental material available online with this article; <https://doi.org/10.1172/jci.insight.96902DS1>). BLT1 is

Conflict of interest: FS and TY have a US patent application (no. 15/525,660) regarding a BLT1 antagonist or a LTB₄ biosynthesis inhibitor as a new preventive or therapeutic agent for AMD.

Submitted: August 22, 2017

Accepted: August 7, 2018

Published: September 20, 2018

Reference information:

JCI Insight. 2018;3(18):e96902.

<https://doi.org/10.1172/jci.insight.96902>.

insight.96902.

expressed by various leukocyte subsets, including granulocytes (neutrophils and eosinophils), monocytes, macrophages, DC, differentiated T cells (Th1, Th2, Th17, and effector CD8⁺ T cells), mast cells, and osteoclasts (10). As shown by previous reports, the LTB₄-BLT1 axis regulates inflammatory and immunological responses such as peritonitis (11), bronchial asthma (12, 13), delayed-type hypersensitivity (14), arthritis (15), atherosclerosis (16, 17), multiple sclerosis (18), psoriasis (19), and obesity-associated insulin resistance (20).

Activated macrophages are roughly classified as classically activated (M1-type) or alternatively activated (M2-type) (21). M1 macrophages are induced by pathogen-associated molecular patterns (e.g., LPS) and inflammatory cytokines (e.g., IFN- γ) and defend against invading microbial pathogens such as bacteria, protozoa, and viruses. Several proteins are used as markers to distinguish M1 and M2 macrophages. Inducible NOS (iNOS) is a representative M1 marker (22–25), and costimulatory molecules (CD80 and CD86) and MHC class II are also useful markers for M1 polarization (26–30). M2 macrophages are regulated by Th2 cytokines (e.g., IL-4 and IL-13), antiinflammatory cytokines (e.g., IL-10 and TGF- β), immune complexes, glucocorticoids, and other factors (31), and they are involved in diverse chronic inflammatory diseases such as parasite infections (32), allergies (33), obesity (34, 35), and the proangiogenic responses that occur in cancer (36) and tissue remodeling and repair (37–39). Mannose receptor (MR, CD206), macrophage galactose N-acetyl-galactosamine specific lectin, (Mgl, CD301), programmed cell death 1 ligand 2 (PD-L2, CD273), and PD-L1 (CD274) are well characterized as the cell surface markers (40–44), and Arginase-1, Fizz1, and Ym1 are known as distinct markers (45–48) for M2 polarization. Recently, we and others reported that M2 macrophages recruited to the injured retina make a critical contribution to the pathogenesis of choroidal neovascularization (CNV) in wet AMD (49–53); however, the molecular mechanisms underlying recruitment of M2 macrophages are poorly understood. Here, we show that BLT1 is mainly expressed by M2 macrophages, which are then recruited to laser-induced retinal lesions and produced VEGF-A- in a BLT1-dependent manner. We also show that LTB₄-BLT1 signaling exacerbates CNV in a mouse model of wet AMD by increasing expression of proangiogenic and profibrotic markers. Importantly, we confirm that blockade of LTB₄-BLT1 signaling strongly inhibits CNV.

Results

BLT1 deficiency ameliorates progression of CNV in a mouse model of AMD. Recent reports showed that LTB₄-BLT1 signaling promotes several chronic diseases including fibrosis (54), insulin resistance (55), tumorigenesis (56); however, its role in chronic eye diseases has been poorly understood. To examine the pathological role of BLT1 in the eye in vivo, we performed retinal laser photocoagulation to induce wet AMD (57) in BLT1-WT and BLT1-deficient (BLT1-KO) mice (13) of various ages. BLT1-WT mice showed an age-dependent increase in CNV volume (Figure 1A, upper panels). Surprisingly, aging did not affect CNV development in BLT1-KO mice, and the volume of CNV was much smaller in old BLT1-KO mice than in old BLT1-WT mice (Figure 1A, lower panels). The CNV volume in BLT1-WT mice increased in an age-dependent manner (average volume in young mice, $3.1 \times 10^5 \mu\text{m}^3$; middle-aged mice, $5.4 \times 10^5 \mu\text{m}^3$; and old mice, $7.2 \times 10^5 \mu\text{m}^3$); this was not the case in BLT1-KO mice on day 7 after injury (young mice, $2.6 \times 10^5 \mu\text{m}^3$; middle-aged mice, $2.3 \times 10^5 \mu\text{m}^3$; and old mice, $3.2 \times 10^5 \mu\text{m}^3$) (Figure 1B). We also observed that the size of the laser-induced lesion in old BLT1-KO mice was smaller than that in old BLT1-WT mice; however, the overall retinal structure was the same in both groups (Figure 1C). We also confirmed that BLT1-KO mice had smaller lesion areas than those of BLT1-WT mice in aged eyes (average area in BLT1-WT mice, $3.0 \times 10^4 \mu\text{m}^2$; BLT1-KO mice, $1.3 \times 10^4 \mu\text{m}^2$) (Figure 1D). In wet AMD, pathological angiogenesis is critically involved in CNV development and accelerates subretinal fibrosis by increasing various cytokines and chemokines (2, 58, 59). Consistently, expression of mRNA encoding proangiogenic growth factors *Vegfa*, *Pdgfb*, and *Fgf2* in laser-injured BLT1-KO eyes was approximately half as much as in BLT1-WT eyes on day 7 after laser injury in old mice (Figure 2A, upper panels). The amounts of mRNA encoding inflammatory cytokines (*Il1b* and *Tnf*), endothelial cell markers (*Tek*, also known as *Tie2*, and *Vwf*), and the profibrotic factors *Tgfb1*, *Pdgfb*, and *Fgf2* (59) were lower in laser-treated BLT1-KO eyes. However, expression of mRNA encoding the chemokines *Ccl3* (Figure 2A, middle and lower panels) and *Ccl2* (data not shown), both of which were reported to play a role in AMD pathogenesis (60, 61), was not significantly different between the BLT1-KO and BLT1-WT groups. We previously cloned a low-affinity LTB₄ receptor, BLT2 (62, 63), which is involved in colitis (64), epidermal wound healing (65), and acute lung injury (66), and we examined the effect of BLT2 deficiency in the same AMD model (Supplemental Figure 2). We found that BLT2 was not involved in AMD because the CNV volume in BLT2-KO mice was comparable with that in

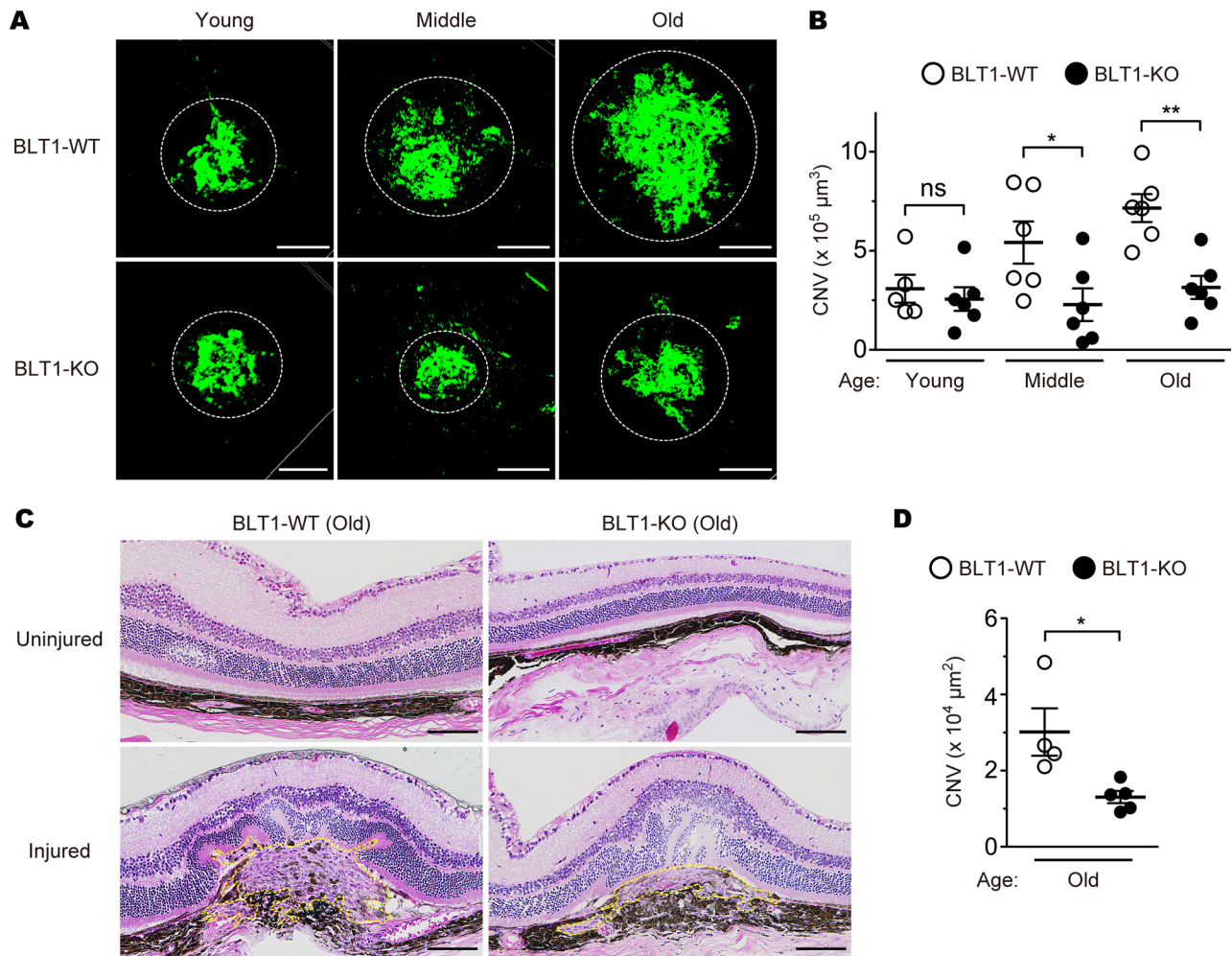


Figure 1. BLT1 deficiency attenuates CNV in a mouse model of AMD. Images of isolectin B₄ (iB₄) staining (**A**) and CNV volume (**B**) in the RPE-choroid complex from the eyes of BLT1-WT (open circles) and BLT1-KO (filled circles) mice after laser-induced injury. Green represents a CNV area positive for iB₄ staining. Mice were grouped by age: young, 8–12 weeks old; middle-aged, 20–24 weeks old; old, 40–48 weeks old. $n = 5$ –6 mice per group. (**C** and **D**) Images of H&E staining (**C**) and CNV lesion area (**D**). H&E staining of the uninjured and laser-injured retinas from aged BLT1-WT and BLT1-KO mice (>40 weeks old). Yellow dotted lines denote the lesion areas. $n = 4$ –5 per group. Scale bar: 100 μm (**A** and **C**). (**B** and **D**) $*P < 0.05$; $**P < 0.01$ (1-way ANOVA with Bonferroni's post hoc test [**B**] and Student's *t* test [**D**]). Results are representative of at least 2 independent experiments.

their WT (BLT2-WT) littermates (BLT2-WT mice, $4.4 \times 10^5 \mu\text{m}^3$; BLT2-KO mice, $3.4 \times 10^5 \mu\text{m}^3$) (Supplemental Figure 2B). Next, we performed the simultaneous quantification of 52 eicosanoids in laser-injured mouse eyes using a liquid chromatography–mass spectrometry (LC-MS/MS) (Figure 2 and Supplemental Figure 3). On days 1 and 3 after laser injury, the amount of LTB₄ (Figure 2B) and 5-hydroxyeicosatetraenoic acid (5-HETE) (Supplemental Figure 3A) in the eyes markedly increased both in young and old mice. These results are consistent with the previous studies showing that various leukotrienes, including LTB₄, were produced from the retinal glial cells, retinal endothelial cells, and RPE in the pathogenesis of inflammatory eye diseases at early phase (67, 68). Taken together, these results suggest that LTB₄-BLT1 signaling is critical for progression of laser-induced CNV.

BLT1 is expressed by macrophages and is involved in CNV development. As BLT1 is highly expressed in various subsets of leukocytes, we speculated that BLT1 expressed in retinal leukocytes is responsible for CNV. Previous studies showed that retinal leukocytes were reconstituted with donor leukocytes by BM transplantation (69–73). To examine whether BLT1-expressing leukocytes play a role in laser-induced CNV, we implanted BLT1-WT or BLT1-KO BM cells from aging donors into lethally irradiated WT mice from aging recipients to generate BM chimeric mice and then examined CNV volume (Figure 3, A and B). We confirmed that more than 90% of BM cells and peripheral blood leukocytes (PBL) of the CD45.2⁺ recipients (C57BL/6J-Ly5.2 mice) were donor-derived CD45.1⁺ cells from a congenic strain (C57BL/6-Ly5.1 mice) (Supplemental

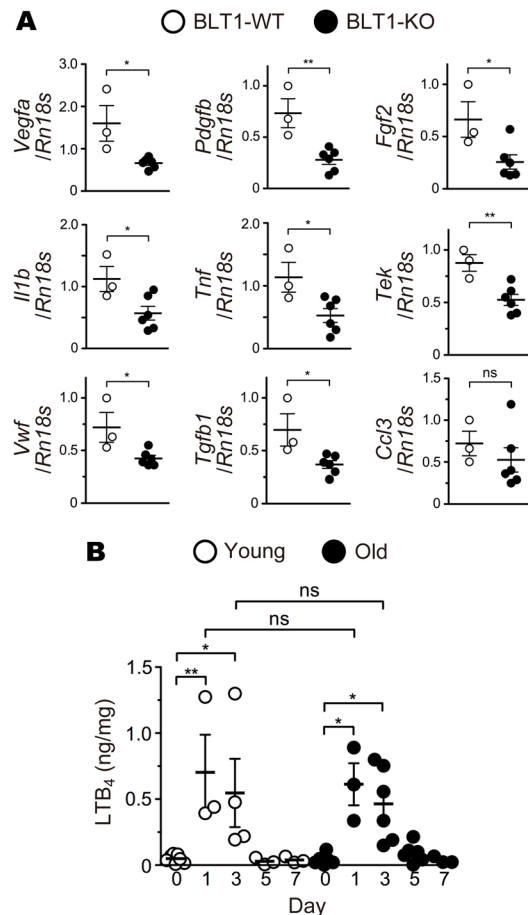


Figure 2. BLT1 deficiency reduces expression of proangiogenic and profibrotic factors in the laser-induced eyes. (A) Quantitative PCR analysis of mRNA for various proangiogenic and profibrotic factors, cytokines, and chemokines in the eyes from aged BLT1-WT (white) and BLT1-KO (black) mice (>20 weeks old) on day 7 after laser injury. $n = 3-6$ per group. (B) Time-dependent changes in LTB_4 content in laser-injured eyes from young (white) and old (black) WT mice (young, 8 weeks old; old, >20 weeks old). $n = 3-7$ per group. * $P < 0.05$; ** $P < 0.01$ (Student's t test [A] and 1-way ANOVA with Bonferroni's post hoc test [B]). Results are representative of at least 2 independent experiments.

Figure 4, A and B). These results showed that the efficiency of BM transplantation is independent of the age of donors or recipients (Supplemental Figure 4, C and D). The volume of CNV in BLT1-KO chimeras was significantly smaller than that in BLT1-WT chimeras (BLT1-WT BM into WT, $10.3 \times 10^5 \mu\text{m}^3$; BLT1-KO BM into WT, $6.8 \times 10^5 \mu\text{m}^3$) (Figure 3B). We further analyzed the numbers and the percentages of leukocyte populations in the eyes by FACS analysis (Figure 3, C and D). $CD45^+$ total leukocytes and $CD11b^{\text{hi}}F4/80^{\text{lo}}Ly6G^{\text{hi}}$ neutrophils peaked at day 1, but $CD11b^{\text{hi}}F4/80^{\text{lo}}Ly6C^{\text{hi}}$ inflammatory monocytes and $CD11b^{\text{hi}}F4/80^{\text{hi}}$ macrophages peaked at day 3 after laser injury in the eyes of aged WT mice. Consistent with the previous studies, we found that BLT1 is abundantly expressed in $CD11b^{\text{hi}}F4/80^{\text{lo}}Ly6G^{\text{hi}}$ neutrophils and $CD11b^{\text{hi}}F4/80^{\text{hi}}$ macrophages in the laser-injured eyes (data not shown). We further observed that BLT1 $^+$ macrophages infiltrated the periphery of the laser-injured area in the RPE-choroid in aged mice on day 5 after laser injury (Figure 3E, upper panels) but not in young mice (Figure 3E, lower panels). To determine whether BLT1 $^+$ macrophages contribute to the development of CNV, we next depleted macrophages by IVI of clodronate liposomes (Figure 4 and Supplemental Figure 5) as previously described (74). IVI of clodronate liposomes significantly reduced $F4/80^+$ macrophages in the RPE-choroid compared with control liposomes (Supplemental Figure 5C) but did not affect the number of DAPI $^+$ cells (Supplemental Figure 5D). Macrophage depletion reduced CNV volume in BLT1-WT mice (control, $13.5 \times 10^5 \mu\text{m}^3$; clodronate, $2.6 \times 10^5 \mu\text{m}^3$) to levels observed in BLT1-KO mice (control, $2.5 \times 10^5 \mu\text{m}^3$; clodronate, $1.1 \times 10^5 \mu\text{m}^3$) (Figure 4B). Taken together, these results suggest that BLT1 $^+$ macrophages exacerbate laser-induced CNV.

BLT1 is expressed in M2 macrophages in vitro and in vivo. Recent studies have been shown that macrophages are skewed toward proangiogenic phenotype in the injured tissue or the tumor microenvironment (36, 39, 44, 48, 53, 75). Next, we examined BLT1 expression in M1 and M2 macrophages using BM-derived macrophages (BMDMs) (Figure 5, A and B, and Supplemental Figure 6A), RAW264.7 cells (mouse monocyte/macrophage cell line) (Figure 5C), and THP-1 cells (human monocytic cell line) (Figure 5D). M2 polarization of BMDMs induced BLT1 mRNA (*Ltb4r1*) (Figure 5A and Supplemental Figure 6A, M2) and protein (Figure 5B, M2) expression, while M1 polarization or nonpolarized M0 BMDMs showed lower levels of

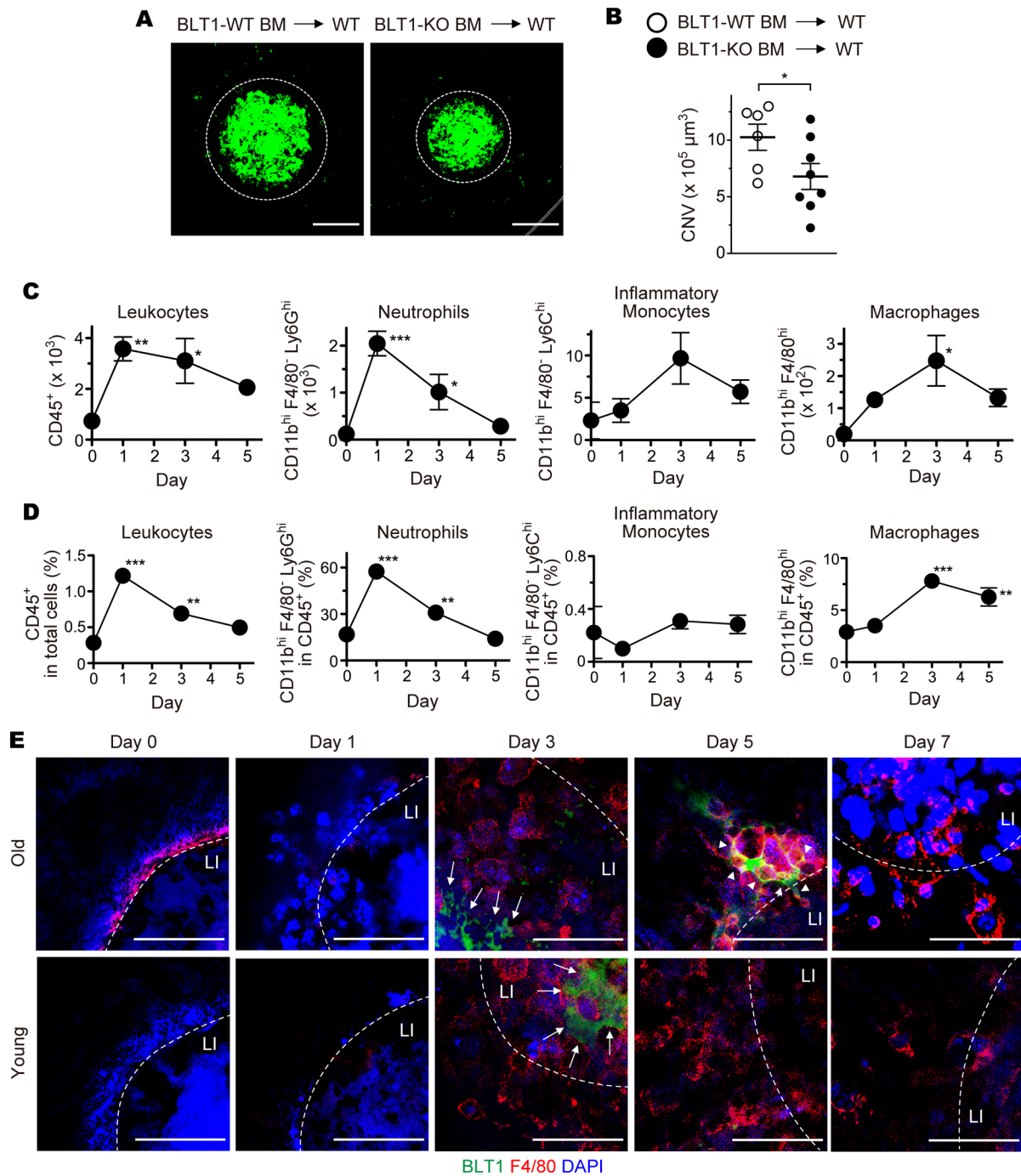


Figure 3. BLT1-expressing macrophages are recruited to the periphery of laser-induced CNV. Images of iB_4 staining (A) and CNV volume (B) in the RPE-choroid of chimeric mice receiving BM cells from aged BLT1-WT (white) or BLT1-KO (black) mice (>20 weeks old). $n = 6-8$ mice per group. (C and D) Flow cytometry analysis of cells isolated from the laser-injured eyes of aged WT mice (>20 weeks old). The populations of the leukocytes are gated as follows: total leukocytes, $CD45^+$; neutrophils, $CD11b^{hi}F4/80^-Ly6G^+$; inflammatory monocyte, $CD11b^{hi}F4/80^-Ly6C^+$; macrophages, $CD11b^{hi}F4/80^{hi}$. The numbers (C) and percentages (D) of the leukocyte populations were analyzed on days 1, 3, and 5 after laser injury. Day 0 refers to a sample taken from uninjured eyes. $n = 3-4$ per group. (E) Immunofluorescence staining of the laser-injured RPE-choroids from WT mice (young, 8 weeks old; old, >20 weeks old) with anti-F4/80 (red) and -BLT1 (green) mAbs. Nuclei were visualized with DAPI (blue). LI (white dotted lines) denotes the location of laser injury. White arrows show F4/80-negative and BLT1-positive cells. White arrowheads show F4/80- and BLT1-double positive cells. Scale bar: $100\ \mu m$ (A) or $50\ \mu m$ (E). (B) $*P < 0.05$ (Student's t test). (C and D) $*P < 0.05$; $**P < 0.01$; $***P < 0.005$ versus Day 0 (1-way ANOVA with Dunnett's post hoc test). Results are representative of at least 2 independent experiments.

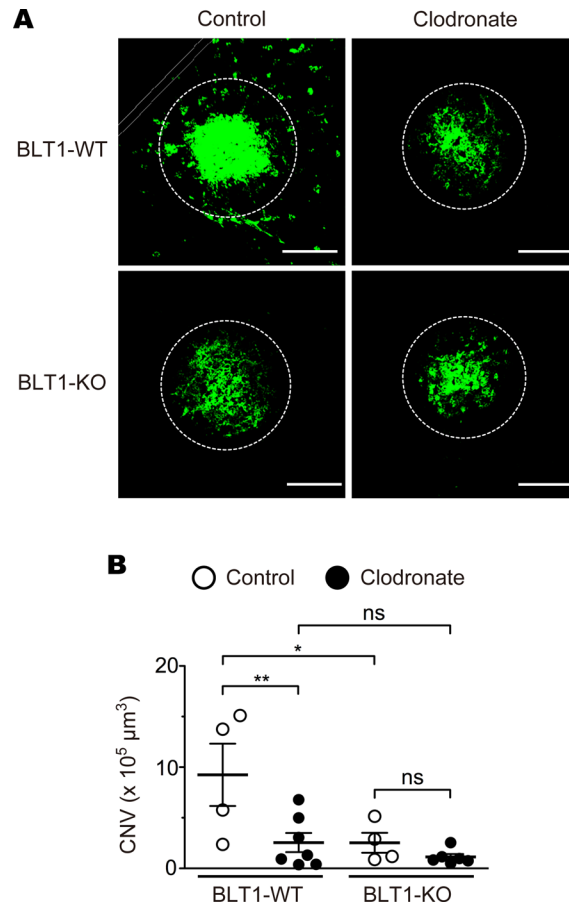


Figure 4. BLT1-expressing macrophages are involved in the pathogenesis of laser-induced CNV. (A and B) The effect of clodronate liposome-mediated macrophage depletion (indicated as Clodronate, filled circles) on CNV volume in aged BLT1-WT and BLT1-KO mice (>20 weeks old). Control refers to control liposomes (open circles). $n = 4-7$ mice per group. Scale bar: 100 μm . (B) * $P < 0.05$; ** $P < 0.01$ (1-way ANOVA with Newman-Keuls post hoc test). Results are representative of at least 2 independent experiments.

BLT1 expression (Figure 5, A and B, and Supplemental Figure 6A, M0 and M1). Polarization of BMDMs was confirmed by examining the expression levels of mRNA for M2-specific markers including CD206 (*Mrc1*), CD301b (*Mgl2*), PD-L2 (*Pdcd1lg2*), Arginase-1 (*Arg1*), Fizz1 (*Retnla*), and Ym1 (*Chil3*) (Supplemental Figure 6, B–G) or an M1 specific marker, iNOS (*Nos2*) (Supplemental Figure 6H). Consistent with these results, M2-polarization induced BLT1 expression in both RAW264.7 and THP-1 cells, and M1- or M0-polarization did not (Figure 5, C and D, left panels). Expression of PD-L2 and CD80 proteins also confirmed the proper M2 and M1 polarization, respectively (Figure 5, C and D, middle and right panels). In addition, we analyzed the number and percentage of M2 macrophages by FACS analysis (Figure 5, E–H). The absolute number of CD206⁺ M2 macrophages peaked at day 3 after laser injury (Figure 5E), but the percentage of CD206⁺ M2 macrophages in CD45⁺ total leukocytes (Figure 5F) or in CD11b^{hi}F4/80^{hi} total macrophages (Figure 5G) peaked at day 5 in the eyes of aged WT mice. The percentage of BLT1⁺CD206⁺ M2 macrophages was significantly higher during days 1–5 after laser injury in aged mice (Figure 5H). We also found that ocular-infiltrating BLT1⁺ macrophages expressed high levels of several M2 markers (CD206, CD301, and PD-L2) on day 5 after laser injury (Figure 5I). Interestingly, the expression levels of the M2 markers on BLT1⁺ macrophages were slightly higher than those on BLT1⁻ macrophages (Figure 5I, lower panels). To note, we found that BLT1 expression (Figure 5, J and K) in aged mice were higher than those in young mice in the ocular-infiltrating CD206⁺ M2 macrophages on day 3 after laser injury. These results suggest that the infiltration of ocular M2 macrophages is accelerated by age-dependent upregulation of BLT1.

The LTB₄-BLT1 axis upregulates recruitment of M2 macrophages and subsequent VEGF-A production. Although some molecules and signaling pathways have been implicated in the activation of M2 macrophages, the cellular and molecular mechanism is not fully elucidated. In general, BLT1 mediates LTB₄-induced calcium mobilization, chemotaxis, and inhibition of adenylyl cyclase through the activation of Gq and Gi proteins (76). To determine whether M2 macrophages express functional BLT1 in vitro, we performed calcium mobilization (Figure 6A) and chemotaxis (Figure 6, B–D, and Supplemental Videos 1 and 2) assays. M2-polarized, but not M1- or M0-polarized, RAW264.7 cells exhibited increased intracellular calcium

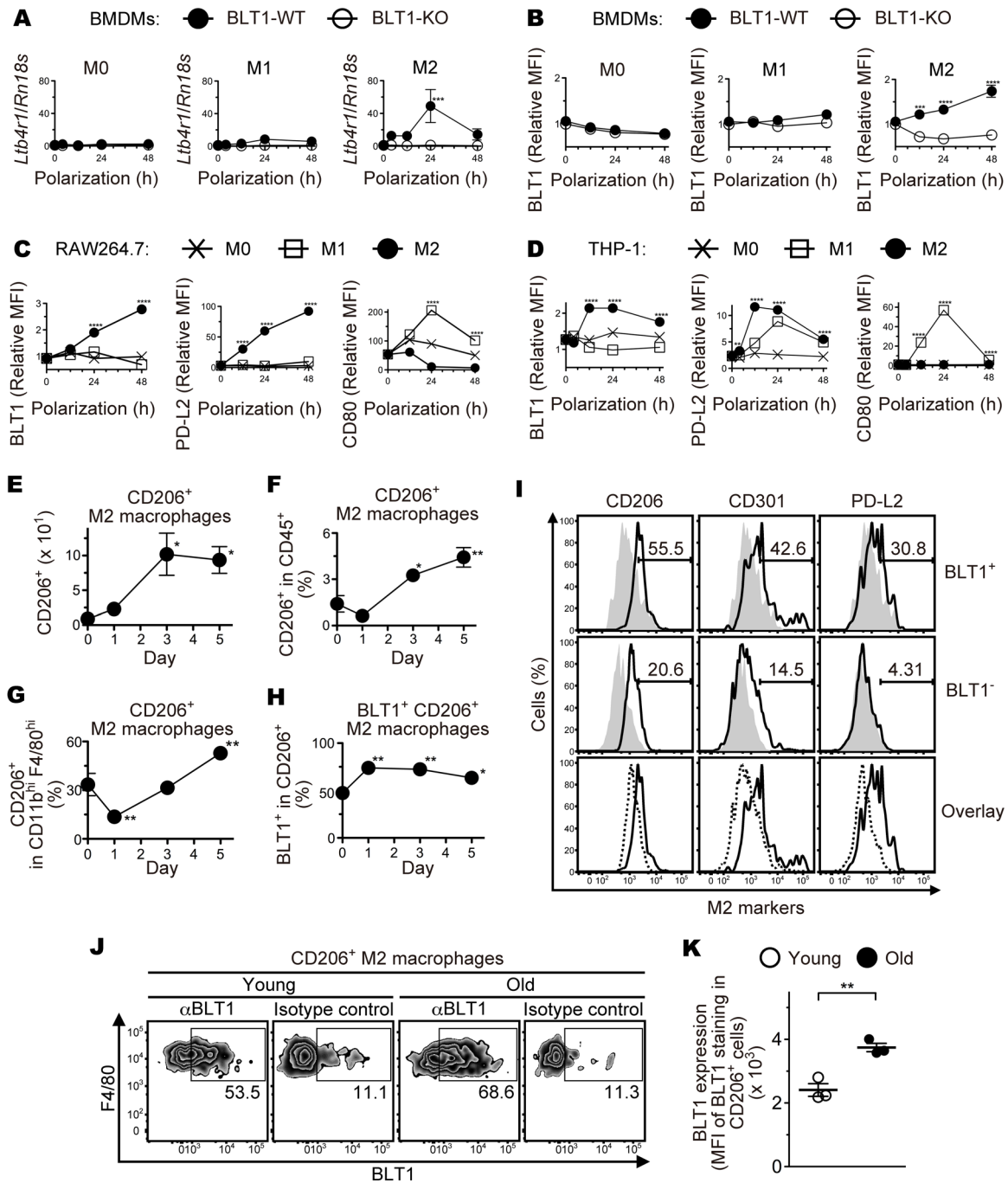


Figure 5. M2-type macrophages express BLT1 and infiltrate into the injured eyes of aged mice. BMDMs from aged BLT1-WT (filled circles) and BLT1-KO (open circles) mice (>20 weeks old) were polarized to M1 and M2 macrophages, and BLT1 expression was examined by quantitative PCR (A) and Flow cytometry analysis (B). M0 denotes a sample of nonpolarized BMDMs. RAW264.7 (C) and THP-1 (D) cells were polarized to M0 (cross plots), M1 (open squares), and M2 (filled circles) macrophages, and expression of BLT1, PD-L2 (an M2 marker), and CD80 (an M1 marker) was examined by flow cytometry. The y axis shows the MFI relative to that of an isotype control (mouse IgG₁). MFI, mean fluorescence intensity. *n* = 3 per group. (E-H) FACS analysis of M2 macrophages isolated from the laser-injured eyes of aged WT mice (>20 weeks old) as described in Figure 3, C and D. CD206⁺ M2 macrophages, CD11b^{hi}F4/80^{hi}CD206⁺; CD206⁺BLT1⁺M2 macrophages, CD11b^{hi}F4/80^{hi}CD206⁺BLT1⁺. *n* = 3–4 per group. (I) FACS analysis of M2 markers on the ocular-infiltrating BLT1⁺ and BLT1⁻ macrophages on day 5 after laser injury from aged WT mice. CD206, CD301, and PD-L2 are specific surface markers of M2 macrophages. Cells were stained with anti-CD206, anti-CD301, and anti-PD-L2 mAbs (black outlines) or isotype controls (gray filled histograms). Overlays show the expression level of M2 markers on BLT1⁺ (black outlines) and BLT1⁻ (black dotted lines) macrophages. These macrophages were gated as the CD45⁺F4/80^{hi}CD11b^{hi} population. (J and K) FACS analysis of BLT1 expression on the ocular-infiltrating CD206⁺ M2 macrophages on day 3 after laser injury from young or aged WT mice. *n* = 3 per group. (A-D) ***P* < 0.01; ****P* < 0.005; *****P* < 0.001 versus 0 hours (2-way ANOVA with Bonferroni's post hoc test). (E-H) **P* < 0.05; ***P* < 0.01 versus day 0 (1-way ANOVA with Dunnett's post hoc test). (K) ***P* < 0.01 (Student's *t* test). Results are representative of at least 2 independent experiments (A-I).

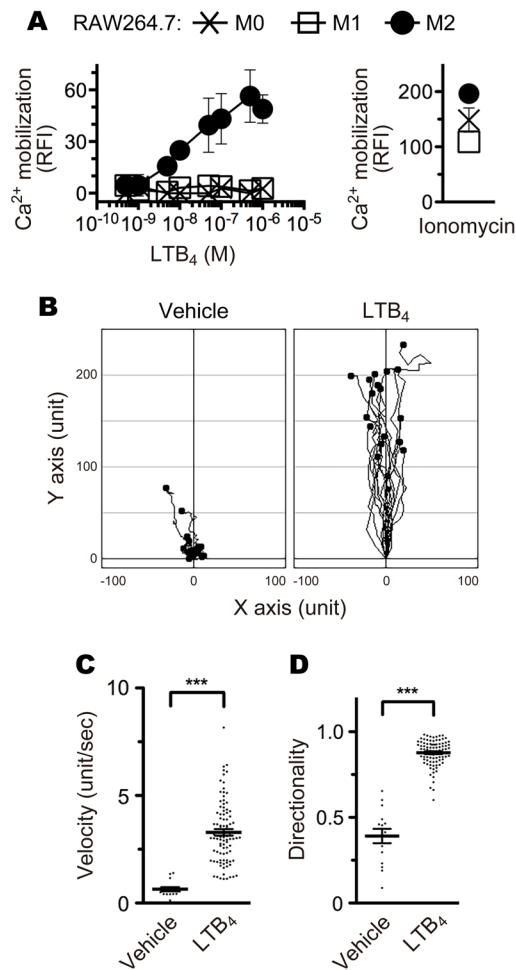


Figure 6. M2 macrophages respond to LTB₄. (A) Calcium mobilization in M0- (cross plots), M1- (open squares), and M2- (filled circles) RAW264.7 cells after stimulation with the indicated concentrations of LTB₄ and 2 μM ionomycin. *n* = 3 per group. (B) Chemotaxis of M2-RAW264.7 cells toward 100 nM (highest concentration) of LTB₄ (*n* = 18) or vehicle (*n* = 15). The velocity (C) and directionality (D) of M2-RAW264.7 cell migration in the presence of vehicle (*n* = 15) or 100 nM LTB₄ (*n* = 93) are shown. (C and D) ****P* < 0.005 (Student's *t* test). Results are representative of at least 2 independent experiments.

mobilization upon LTB₄ stimulation (Figure 6A) and migrated along an increasing LTB₄ concentration gradient (Figure 6B and Supplemental Videos 1 and 2). The M2-RAW264.7 cells significantly responded to LTB₄ with a velocity and directionality of 3.29 unit s⁻¹ and 0.88, respectively (Figure 6, C and D). We next analyzed the expression levels of VEGF-A mRNA (Figure 7A) and protein (Figure 7B) in M2 BMDMs from BLT1-WT and BLT1-KO mice. Stimulation of LTB₄ significantly induced VEGF-A mRNA and protein expression in M2 BMDMs from BLT1-WT but not in BLT1-KO M2 BMDMs. Thus, LTB₄-BLT1 signal is important for activation of M2 macrophages.

M2 macrophages promote BLT1-mediated development of CNV. Recent findings have experimentally confirmed that adoptive transferred M2 macrophages develop CNV by stimulating an abnormal angiogenesis (52, 77–79). To clarify whether BLT1⁺ M2 macrophages exacerbate CNV, we adoptively transferred M0, M1, and M2 macrophages from BLT1-WT or BLT1-KO mice into laser-injured WT mice (Figure 8). Adoptive transfer of BLT1-WT M2-BMDMs resulted in marked CNV formation when compared with transfer of BLT1-KO M2-BMDMs (BLT1-WT M2 into WT, 10.5 × 10⁵ μm³; BLT1-KO M2 into WT, 4.4 × 10⁵ μm³); adoptive transfer of M0- and M1-BMDMs has little effect on CNV formation (BLT1-WT M0, 2.9 × 10⁵ μm³; BLT1-KO M0, 2.1 × 10⁵ μm³; BLT1-WT M1, 2.7 × 10⁵ μm³; BLT1-KO M1, 1.6 × 10⁵ μm³) (Figure 8, A and B). Histological analysis revealed that BLT1-WT M2-injected eyes developed more robust neovascularization in retinal and choroidal tissues than BLT1-KO M2-injected eyes (BLT1-WT M2 into WT, 2.8 × 10⁴ μm²; BLT1-KO M2 into WT, 1.0 × 10⁴ μm²) (Figure 8, C and D). Thus, expression of BLT1 is required for M2-induced CNV.

Pharmacological inhibition of LTB₄-BLT1 signaling ameliorates CNV development. Several studies demonstrated that a BLT1 antagonist CP105696 completely blocked [³H]-labeled LTB₄ binding (IC₅₀ of 3.7 nM for human neutrophils) (80), calcium mobilization (0.1–1 μM for human neutrophils) (81), phagocytosis (1 μM for BMDMs) (82), and chemotaxis (0.1 μM for mouse peritoneal macrophages) (20) by antagonizing BLT1.

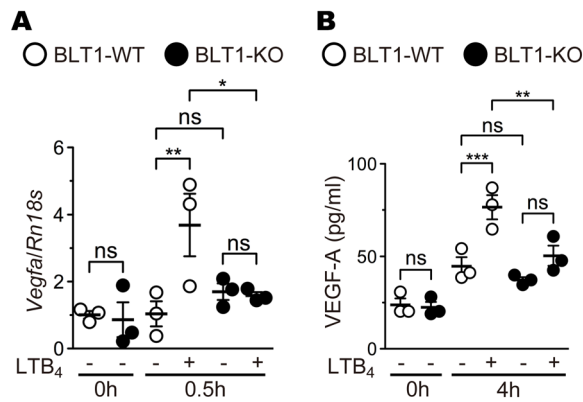


Figure 7. LTB₄-BLT1 signaling induces VEGF-A production in M2 macrophages. BMDMs from aged BLT1-WT (open bars) and BLT1-KO (filled bars) mice (>20 weeks old) were polarized to M2 macrophages and were stimulated with 500 nM LTB₄ or vehicle for 0.5 hours (A) or 4 hours (B). The expression levels of VEGF-A mRNA (A) and protein (B) were measured by quantitative PCR and ELISA. *n* = 3 per group. (A and B) **P* < 0.05; ***P* < 0.01; ****P* < 0.005 (1-way ANOVA with Newman-Keuls post hoc test). Results are representative of at least 2 independent experiments.

To investigate whether blockade of LTB₄-BLT1 signaling (Supplemental Figure 1) (9, 83, 84) attenuates CNV, we treated mice by IVI of CP105696, prior to laser-induced injury (Figure 9, A and C, upper panels). We also tested the effects of 3 inhibitors of LTB₄-producing enzymes: zileuton, a specific inhibitor of 5-LO; MK-886, a specific inhibitor of FLAP; and bestatin, an inhibitor of LTA₄H (Figure 9A, lower panels, and Figure 9C, middle and lower panels). CP105696 caused a dose-dependent reduction in CNV volume (DMSO, $6.6 \times 10^5 \mu\text{m}^3$; CP105696, 0.2 pmol [$3.5 \times 10^5 \mu\text{m}^3$], 2 pmol [$2.0 \times 10^5 \mu\text{m}^3$], 20 pmol [$1.0 \times 10^5 \mu\text{m}^3$]) (Figure 9B) and in CNV lesion area (DMSO, $3.5 \times 10^4 \mu\text{m}^2$; CP105696, 20 pmol [$1.6 \times 10^4 \mu\text{m}^2$]) (Figure 9D). The CNV development was also inhibited by treatment with zileuton, MK-886, or bestatin (CNV volume: zileuton, $2.8 \times 10^5 \mu\text{m}^3$; MK-886, $2.8 \times 10^5 \mu\text{m}^3$; bestatin, $1.9 \times 10^5 \mu\text{m}^3$) (CNV lesion area: zileuton, $1.3 \times 10^4 \mu\text{m}^2$; MK-886, $1.8 \times 10^4 \mu\text{m}^2$; bestatin, $1.4 \times 10^4 \mu\text{m}^2$) (Figure 9, B and D). Moreover, we confirmed that CP105696 suppressed the infiltration of CD206⁺ M2 macrophages and BLT1⁺CD206⁺ M2 macrophages (Figure 9, E and F).

Given that some of these drugs are orally available, the LTB₄-BLT1 axis may become a novel therapeutic target for laser-induced CNV.

Discussion

Here, we demonstrate that the volume of CNV in BLT1-WT mice, but not in BLT1-KO mice, increased in an age-dependent manner (Figure 1). A high-affinity LTB₄ receptor, BLT1, which was expressed in ocular-infiltrating macrophages (Figure 3E) was responsible for CNV (Figure 4 and 8). On the other hands, a low-affinity LTB₄ receptor, BLT2, which is ubiquitously expressed in human and mouse tissues (85) including cornea and conjunctiva (86), was not involved in laser injury-induced CNV because there was no significant difference in CNV volume and histology between BLT2-WT and BLT2-KO mice (Supplemental Figure 2). As we reported recently, M2-type macrophages are important for the development of CNV after laser injury (53); here, we also demonstrate that ocular-infiltrating M2 macrophages contributed to CNV development via LTB₄-BLT1 signaling pathway. Indeed, laser-induced injury increased the amount of LTB₄ in the eyes (Figure 2B), which then attracted BLT1⁺ M2 macrophages to the injured mouse retina (Figure 5, E–K). We also found that BLT1 was only induced during M2 polarization of primary mouse macrophages (Figure 5, A and B) and mouse (Figure 5C) or human (Figure 5D) macrophage cell lines. Preliminary experiments with a STAT3 selective inhibitor suggest that, of these, the IL-10/JAK1/STAT3 signaling pathway is likely critical for induction of BLT1 expression (Supplemental Figure 7). Recent studies show that expression of IL-10 and M2 markers (e.g., CD163 and Arginase-1), but not M1 markers (e.g., IL-6 and TNF- α), is increased in senescent macrophages, thereby promoting CNV development (51, 52). Therefore, we expected that BLT1 expression is also increased in senescent M2 macrophages in the eyes of older mice. We actually found that the BLT1 expression of M2 macrophages in the older eyes was higher than that in the younger eyes after induction of laser injury (Figure 5, J and K). The elevated BLT1 could accelerate LTB₄-dependent recruitment of M2 macrophages to CNV lesions, leading to the production of various

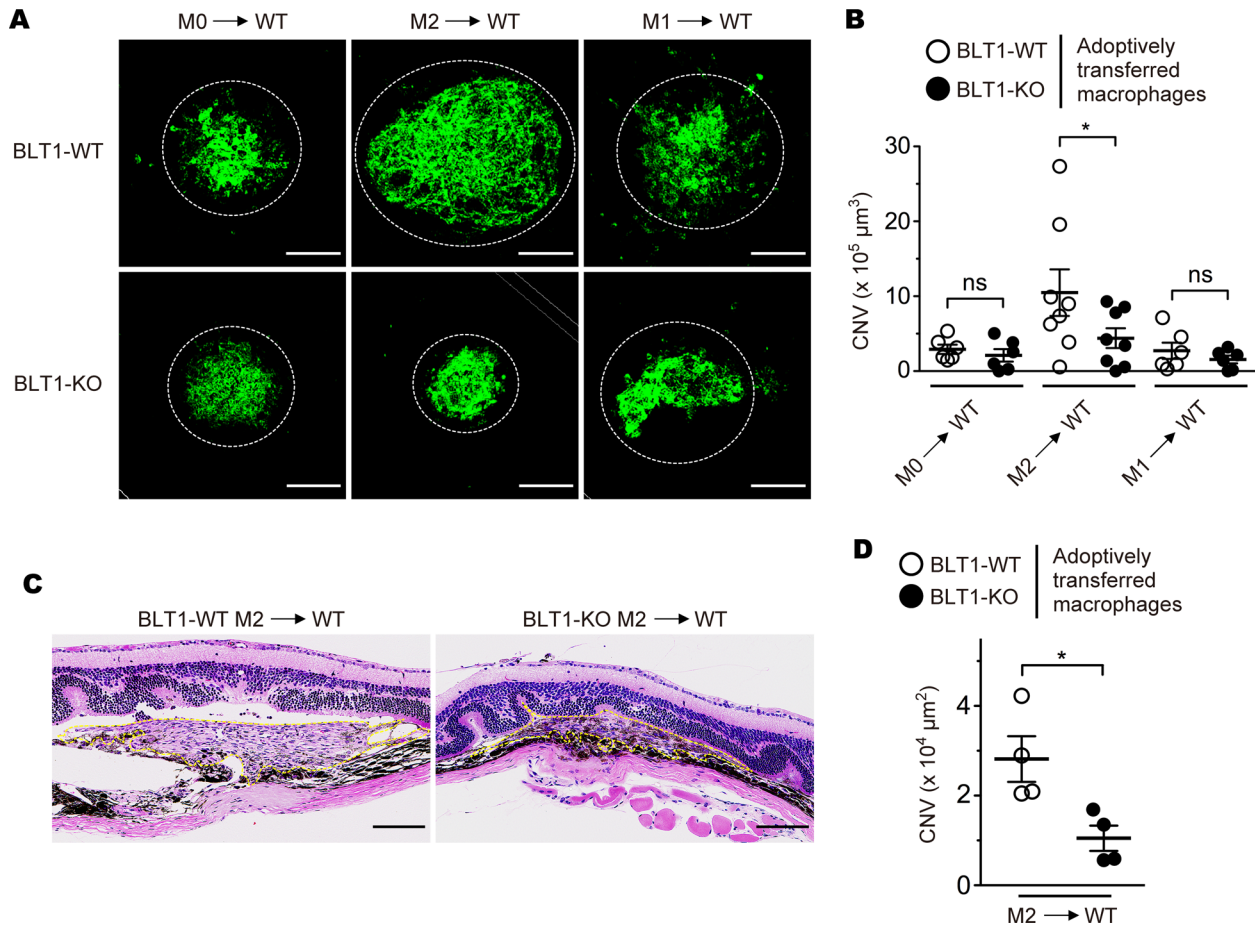


Figure 8. M2 macrophage-dependent CNV development requires BLT1. Images of iB_4 staining (**A**) and CNV volume (**B**) in the RPE-choroid of recipient mice that received M0-, M2-, and M1-BMDMs from aged BLT1-WT (open circles) or BLT1-KO (filled circles) mice (>20 weeks old). $n = 6-8$ mice per group. (**C** and **D**) H&E staining of the laser-injured retinas of recipient mice receiving M2-BMDMs from BLT1-WT or BLT1-KO mice (>20 weeks old). Yellow dotted lines show the lesion area. $n = 4$ per group. Scale bar: 100 μm (**A** and **C**). (**B** and **D**) $*P < 0.05$ (1-way ANOVA with Bonferroni's post hoc test [**B**] and Student's t test [**D**]). Results are representative of at least 2 independent experiments.

proangiogenic factors, including VEGF-A through the activation of BLT1 (Figure 7). Such chain of events would also promote human CNV in wet AMD.

The findings presented herein might contribute to the development of novel anti-AMD drugs (Figure 9). Although anti-VEGF agents (e.g., ranibizumab and bevacizumab) are clinically and commercially available for wet AMD (87), several clinical trials have examined new therapeutic agents that targeting components of the VEGF (e.g., VEGF receptor tyrosine kinases) or other signaling pathways (e.g., PDGF) (88). To date, the LTB_4 -BLT1 axis has not been examined in AMD. We speculate that agents that target the LTB_4 -BLT1 axis might become useful treatment options for human patients with severe wet AMD. In fact, we examined the BLT1 expression in the diabetic human donor eyes (early progressive diabetic retinopathy, age 55, female) compared with nondiabetic human donor eyes (car accident, age 13, male) (data not shown). We found that BLT1⁺ cells infiltrated into the periphery of the macular drusen, a common early sign of AMD, and choroidal capillaries in the RPE-choroid of diabetic human eyes but not in nondiabetic human eyes. Recent studies show that infiltrated macrophages exhibit M2-phenotype, which accelerate neovascularization to promote tissue repair in the injured retina of retinopathy (38, 79, 89, 90). Hence, the BLT1 may be a promising therapeutic target for CNV of several diseases, including wet AMD. The 5-LO inhibitor zileuton is clinically used as an antiasthmatic drug worldwide (83), and the LTA_4H inhibitor Ubenimex (bestatin) is a chemotherapy agent in Japan (84), with known safety profiles in both cases. This allows their potential off-label use as therapeutic agents for wet AMD, thereby ensuring patient safety. In contrast, MK-886 and CP105696 are not used clinically; thus, more effective and safe inhibitors of FLAP, and antagonists of BLT1, are required.

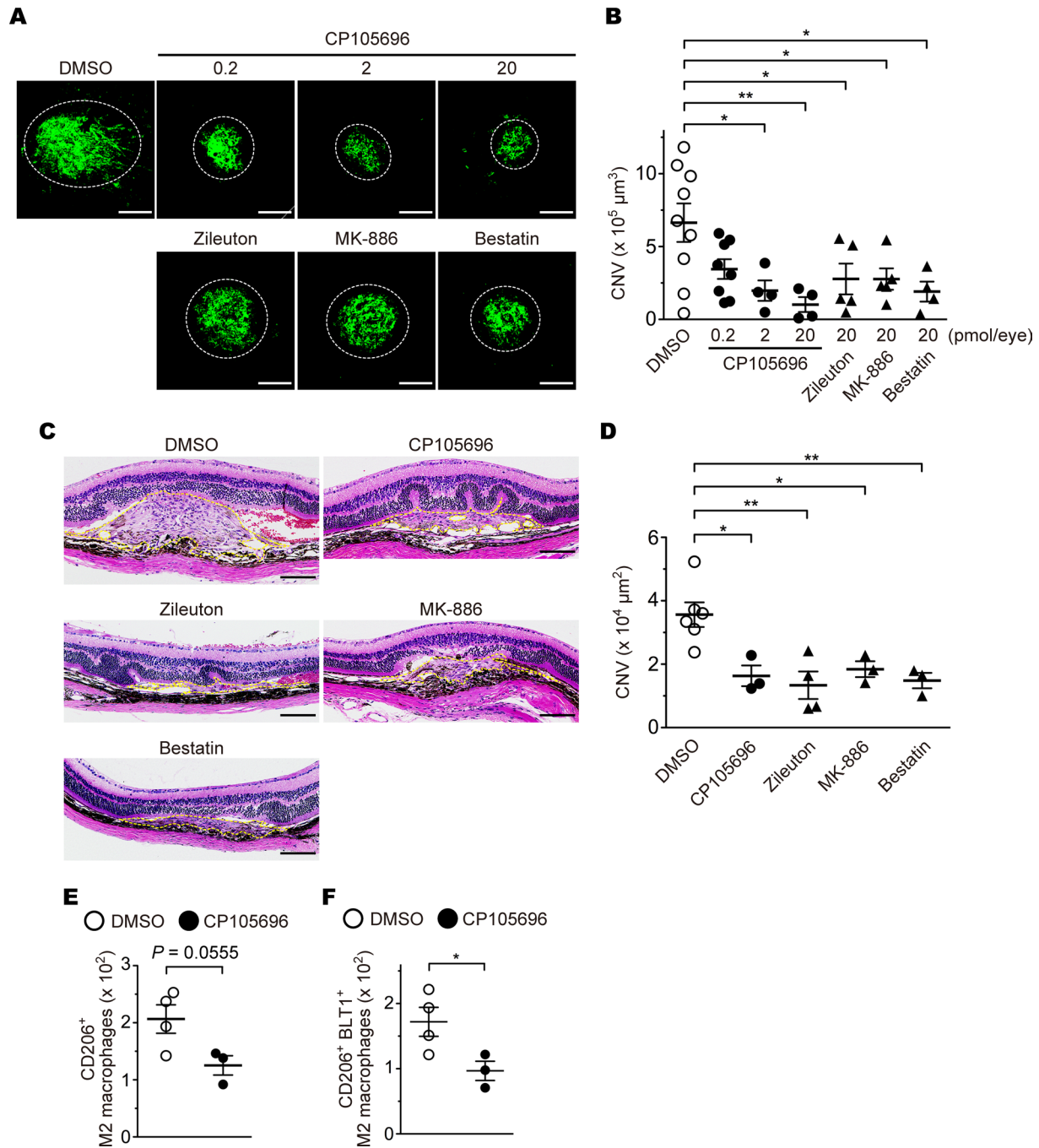


Figure 9. The effects of a BLT1 antagonist and LTB₄ synthesis inhibitors on development of CNV. Images of iB₄ staining (**A**) and CNV volume (**B**) in the RPE-choroid from aged WT mice (>20 weeks old) after administration of 0.2–20 pmol of CP105696 (a BLT1 antagonist; filled circles) or 20 pmol of zileuton (a 5-LO inhibitor), MK-886 (a FLAP inhibitor), or bestatin (a LTA₄H inhibitor) (filled triangles), or vehicle (open circles). *n* = 4–9 mice per group. (**C** and **D**) Images of H&E staining (**C**) and CNV lesion area (**D**). H&E staining of the retinas after aged WT mice (>20 weeks old) with laser-induced injury were treated with CP105696, zileuton, MK-886, and bestatin (20 pmol/eye) or DMSO. Yellow dotted lines show the lesion area. *n* = 3–6 per group. (**E** and **F**) The number of the ocular-infiltrating CD206⁺ or CD206⁺BLT1⁺ M2 macrophages was analyzed on day 3 after laser injury from CP105696- (20 pmol/eye) or DMSO-injected WT mice (> 20 weeks old). *n* = 3–4 per group. Scale bar: 100 μm (**A** and **C**). **P* < 0.05; ***P* < 0.01 (1-way ANOVA with Dunnett’s post hoc test [**B** and **D**] and Student’s *t* test [**E** and **F**]). Results are representative of at least 2 independent experiments (**A–D**).

In conclusion, LTB₄ was found to be a key mediator that attracted M2 macrophages to the laser-injured retinas via BLT1, thereby increasing the severity of CNV. Antagonists of BLT1 or inhibitors of LTB₄ biosynthesis may become novel therapeutic agents to inhibit CNV of wet AMD.

Methods

Animals. BLT1-KO and BLT2-KO mice were generated as previously described (13, 64) and then backcrossed with C57BL/6J mice for more than 12 generations. Aged WT mice (C57BL/6J > 20 weeks old) were purchased from Japan SLC or Kyudo. All mice were maintained in a filtered-air laminar-flow enclosure in a specific pathogen-free facility and given standard laboratory food and water.

Reagents. The selective BLT1 antagonist, CP105696, was from Pfizer. zileuton (a 5-LO inhibitor), MK-886 sodium salt hydrate (a FLAP inhibitor), and bestatin hydrochloride (an inhibitor of aminopeptidases, including LTA₄H) were obtained from MilliporeSigma. LTB₄ was purchased from Cayman Chemical. Unless otherwise noted, all Abs and cytokines were purchased from BioLegend and Peprotech, respectively.

Laser-induced wet AMD model. Mice were anesthetized by i.p. injection of ketamine (100 mg/kg) and xylazine (10 mg/kg), and the pupils were dilated by application of 0.2% tropicamide and 1% phenylephrine hydrochloride (Santen Pharmaceutical Co.). Using a 532-nm laser, a slit-lamp delivery system, and a slide glass as a contact lens, 4 spots (laser power, 200 mW; exposure time, 100 ms; hole size, 75 μm) were placed into each eye. After laser-induced injury and prior to administration of antagonists/inhibitors, the eyes were subjected to IVI of CP105696 (0.2–20 pmol), zileuton (20 pmol), MK-886 (20 pmol), bestatin (20 pmol), or DMSO (vehicle, 0.1%). The volume of the CNV lesions was measured in choroidal flat mounts on day 7 after injury. The anterior segment and retina were removed from the eyecup after fixation in 4% paraformaldehyde in PBS (Wako). The remaining RPE-choroid complex was dehydrated in methanol and stained with 7 μg/ml fluorescein-labeled iB₄ (derived from Griffonia Simplicifolia Lectin I) (Vector Laboratories). After relaxing radial incisions, this complex was flat mounted using mounting medium (Thermo Fisher Scientific) and coverslips. Z-stack images were obtained using a confocal microscope (A1R⁺; Nikon), and the CNV volume was analyzed on reconstructed 3-dimensional images using NIS-Elements (Nikon).

Polarization of M1 and M2 macrophages. BM cells in the femur and tibia were collected from BLT1-WT and BLT1-KO mice (>20 weeks old) and further differentiated in RPMI 1640 (Wako) supplemented with 10% FCS, 100 U/ml penicillin, and 100 μg/ml streptomycin (P/S) (Nacalai) into BMDMs by treatment with 50 ng/ml M-CSF for 3 days. RAW264.7 (a subclone from clone TIB-71) (ATCC) and THP-1 (clone TIB-202) (ATCC) cell lines were maintained in RPMI 1640 supplemented with 10% FCS and P/S. BMDMs and RAW264.7 cells were polarized by exposure to 2 ng/ml mouse IFN-γ and 0.1 μg/ml LPS (MilliporeSigma) (M1) or 20 ng/ml IL-4, IL-10, and IL-13 (from mouse) and 2 ng/ml human TGF-β1 (R&D Systems) (M2) during 48 hours. THP-1 cells were stimulated with 150 nM PMA for 24 hours and then polarized with 2 ng/ml human IFN-γ and 0.1 μg/ml LPS (M1) or 20 ng/ml IL-4, IL-10, and IL-13 (from human) and 2 ng/ml human TGF-β1 (M2) during 48 hours. M0 macrophages were generated by culture in medium without cytokines. All cells were cultured under standard conditions at 37°C and 5% CO₂ in a humidified atmosphere.

H&E staining. Eyes were removed, soaked in 10% buffered formalin solution, embedded in paraffin, sliced (10-μm thickness) using a microtome, and stained with H&E. Images were acquired under a light microscope (BZ-9000; Keyence) and quantified the CNV lesion area using Image J (NIH).

Quantitative PCR (qPCR). Eyecups (the remaining retina, choroid, and RPE from 1–2 eyes) and M0-, M1-, or M2-polarized BMDMs were prepared from BLT1-WT and BLT1-KO mice. For VEGF-A mRNA expression analysis, M2 BMDMs were stimulated with 500 nM LTB₄ or ethanol (as a vehicle control) for 0.5 hours. All samples were treated with TRIzol reagent (Thermo Fisher Scientific) to isolate RNA, according to the manufacturer's instructions. cDNA was synthesized from total RNA with reverse transcriptase and an optimized blend of oligo-dTs and random primers using an QuantiTect Reverse Transcription kit (Qiagen) or qPCR RT Master Mix (Toyobo). Target genes were amplified using a real-time PCR System (Thermo Fisher Scientific), DNA polymerase, SYBR Green I Dye (Thermo Fisher Scientific), and specific primers. Gene expression was normalized to 18S rRNA (*Rn18s*) using the ΔΔCT method. The sequences of the primers are as follows: *Vegfa*: forward, 5'-actggaccctggcttactg-3', and reverse, 5'-tctgctctctctgtcgtg-3'; *Rn18s*: forward, 5'-gcaattattccccatgaacg-3', and reverse, 5'-gggacttaatacaacgaacg-3'; *Pdgfb*: forward, 5'-cggcctgtgactagaagtcc-3', and reverse, 5'-gagcttgaggcgtcttg-3'; *Fgf2*: forward, 5'-cggctctactgcaagaacg-3', and reverse, 5'-tgcttgaggattgtagttgacg-3'; *Il1b*: forward, 5'-tgtaataaagacggcacacc-3', and reverse, 5'-tctctttggtattgcttg-3'; *Tnf*: forward, 5'-tctctcattctgctgttg-3', and reverse, 5'-ggctgggcatagaactga-3'; *Tek*: forward, 5'-cataggaggaaactgttacc-3', and reverse, 5'-gcccccacttctgagctt-3'; *Vwf*: forward, 5'-ccaaggagggtgccaact-3', and reverse, 5'-aaaggaagactctggcaagcta-3'; *Tgfb1*: forward, 5'-tggagcaacatgtggaactc-3', and reverse,

5'-cagcagccggttaccag-3'; *Ccl3*: forward, 5'-tgccttctgtcttctct-3', and reverse, 5'-gtggaatctccggcttag-3'; and *Ltb4r1*: forward, 5'-ctcgagggtgccagcac-3', and reverse, 5'-gacaggcaggtgtctctc-3'.

LC-MS analysis. Eyecups isolated from 5–6 eyes were frozen immediately in liquid nitrogen and stored at -80°C . Samples were homogenized in a tissue disrupter (Automill), and lipids were extracted by incubation in methanol overnight at -20°C followed by centrifuged at $5,000\text{ g}$ for 5 minutes at 4°C . Supernatants were then mixed with 9 volumes of 0.1% formic acid in water, which included deuterium-labeled internal standards (Cayman Chemical). Diluted samples were loaded onto a solid-phase extraction cartridge (Waters) and washed serially with 0.1% formic acid in water, 15% methanol and 0.1% formic acid in water, 0.1% formic acid in water, and petroleum ether. After drying the cartridge, eicosanoids were eluted by centrifugation with $200\ \mu\text{l}$ of 0.1% formic acid in methanol. For reverse phase-HPLC-MS/MS, a Shimadzu liquid chromatography system consisting of four LC-20AD pumps, a SIL-20AC autosampler, a CTO-20AC column oven, a FCV-12AH six-port switching valve, and a TSQ Quantum Ultra triple quadrupole mass spectrometer equipped with an electrospray ionization (ESI) ion source (Thermo Fisher Scientific) were used (91, 92). An aliquot of each sample ($50\ \mu\text{l}$) was injected into the trap column, an Opti-Guard Mini C18 (Optimize Technologies), at a total flow rate of $500\ \mu\text{l}/\text{min}$. Three minutes after sample injection, the valve was switched to introduce the trapped sample to the analytical column, a Capcell Pak C18 MGS3 (Shiseido). Separation of lipids was achieved by a linear gradient using water and acetonitrile containing 0.1% formic acid. The total flow rate was $120\ \mu\text{l}/\text{min}$, the column temperature was set at 46°C , and the LC column eluent was introduced directly into a TSQ Quantum Ultra. All compounds were analyzed in a negative ion polarity mode. Eicosanoids were quantified by multiple reaction monitoring (MRM). The MRM transitions monitored were $m/z\ 335 \rightarrow 195$ for LTB_4 , $m/z\ 624 \rightarrow 272$ for LTC_4 , $m/z\ 495 \rightarrow 177$ for LTD_4 , $m/z\ 319 \rightarrow 115$ for 5-HETE, $m/z\ 339 \rightarrow 197$ for $[\text{H}_4]$ LTB_4 , $m/z\ 629 \rightarrow 272$ for $[\text{H}_5]$ LTC_4 , $m/z\ 500 \rightarrow 177$ for $[\text{H}_3]$ LTD_4 , $m/z\ 327 \rightarrow 116$ for $[\text{H}_8]$ 5-HETE. For accurate quantification, calibration curves were generated for each target eicosanoid using known reference standards and the same isotope-labeled internal standard. Automated peak detection, calibration, and calculation were carried out by the Xcalibur 1.2 software package (Thermo Fisher Scientific).

BM transplantation. BM cells were collected from the both femurs and tibiae of donor BLT1-WT and BLT1-KO (>20 weeks old) and 1×10^7 cells were i.v. injected into lethally irradiated (10 Gy X-rays) male WT recipients (>20 weeks old). At 28 days after transplantation, mice were subjected to laser-induced retinal injury, followed by analysis of CNV development.

Immunofluorescence staining and analysis. RPE-choroid complexes were prepared from WT mice as described above and blocked with 5% BSA/0.5% Triton X-100 (MilliporeSigma) in PBS for 1 hour, followed by staining with $10\ \mu\text{g}/\text{ml}$ anti-BLT1 (clone 7A8; generated in-house) (93) and $5\ \mu\text{g}/\text{ml}$ Alexa Fluor 647-labeled anti-F4/80 (clone BM8) mAbs (BioLegend). After washing with 0.1% Tween in PBS, tissues were incubated with HRP-labeled anti-mouse IgG (500-fold dilution) (Rockland Immunochemicals), followed by Tyramide-Alexa Fluor 488 (100-fold dilution) (Thermo Fisher Scientific). Nuclei were stained with DAPI ($5\ \mu\text{g}/\text{ml}$; MilliporeSigma). Samples were visualized under a confocal microscope (A1R⁺; Nikon).

Flow cytometry analysis. BMDMs and RAW264.7 cells were collected in PBS/2 mM EDTA (pH 7.4) containing 2% FCS (FACS buffer). Fc receptors were then blocked with an anti-CD16/32 ($5\ \mu\text{g}/\text{ml}$; 2.4G2) Ab (Fc blocker). BMDMs were stained with anti-F4/80-FITC ($5\ \mu\text{g}/\text{ml}$; clone BM8), anti-CD11b-allophycocyanin (APC) ($2.5\ \mu\text{g}/\text{ml}$; clone M1/70), and biotin-labeled anti-mouse BLT1 ($5\ \mu\text{g}/\text{ml}$; clone 7A8; generated in-house) Ab (93) or mouse IgG₁ ($5\ \mu\text{g}/\text{ml}$; eBioscience) (as an isotype control). RAW264.7 cells were stained with anti-mouse BLT1 ($5\ \mu\text{g}/\text{ml}$; clone 7A8), anti-PD-L2 ($2.5\ \mu\text{g}/\text{ml}$; clone TY25), anti-CD80 ($2.5\ \mu\text{g}/\text{ml}$; clone 16-10A1), or isotype controls for biotin-labeled anti-mouse Abs (eBioscience). After washing with PBS/EDTA, cells were stained with R-phycoerythrin-conjugated (PE-conjugated) Streptavidin ($0.5\ \mu\text{g}/\text{ml}$; eBioscience). THP-1 cells were collected in FACS buffer, blocked with human Fc blocker (Miltenyi Biotec) and stained with anti-human BLT1 (diluted 1:20; clone 203/14F11) (R&D Systems), anti-PD-L2 ($5\ \mu\text{g}/\text{ml}$; clone 24F.10C12), anti-CD80 ($10\ \mu\text{g}/\text{ml}$; clone 2D10), or an isotype control for PE-labeled anti-human Abs (BioLegend). Cells were analyzed in a flow cytometer (FACSCalibur or LSRFortessa; Becton Dickinson). Eyecups were collected from 4–6 laser-injured eyes as follows: (a) young (8- to 12-week-old) or aged (>20-week-old) WT mice or (b) CP105696- (20 pmol/eye) and DMSO-injected WT mice (> 20 weeks old), and ocular-infiltrating cells were isolated using Collagenase D (Roche Diagnostics) in RPMI 1640 as previously described (94). Cells were then incubated with mouse Fc blocker, followed by staining with anti-CD45-FITC ($2.5\ \mu\text{g}/\text{ml}$; clone

30-F11; Becton Dickinson), anti-Ly6G-PE/Cy7 (2.5 µg/ml; clone 1A8), anti-Ly6C-APC/Cy7 (2.5 µg/ml; clone HK1.4), anti-F4/80-Brilliant Violet 421 (2.5 µg/ml; clone BM8), anti-CD11b-Brilliant Violet 510 (5 µg/ml; clone M1/70), and anti-mouse BLT1-APC (5 µg/ml; clone 7A8; generated in-house) Abs in addition to 2.5 µg/ml anti-PD-L2 (clone TY25; BioLegend), 10 µg/ml anti-CD301 (clone ER-MP23; Bio-Rad), 10 µg/ml anti-CD206 (clone MR5D3; BioLegend) biotin-conjugated Abs or isotype controls. Cells were washed and stained with 0.5 µg/ml Streptavidin-PE and were analyzed in a flow cytometer (FACSVerse; Becton Dickinson). For all experiments, dead cells were excluded after staining with 7AAD (Becton Dickinson).

Liposome-mediated depletion of macrophages. Aged BLT1-WT and BLT1-KO mice (>20 weeks old) received an IVI of 90 µg clodronate liposomes (including 16 µg of clodronic acid; injection volume, 2 µl/eye) (Katayama Chemical Industries) or control liposomes after laser-induced injury. RPE-choroid complexes were prepared as described above, stained with Alexa 647-labeled anti-F4/80 mAb or rat IgG_{2a} (as an isotype control), and then nuclei were visualized with DAPI. F4/80⁺ macrophages and DAPI⁺ cells per field were counted using ImageJ.

Adoptive transfer of macrophages. Aged WT mice received M0, M1, and M2 BMDMs (1×10^5 cells in PBS/eye; injection volume, 2 µl/eye) from aged BLT1-WT or BLT1-KO mice (>20 weeks old) via IVI after laser-induced injury.

Calcium mobilization assay. RAW264.7 cells were incubated for 60 minutes with HBSS-based loading buffer containing 20 mM HEPES (pH 7.4) (Thermo Fisher Scientific), 2.5 mM Probenecid (MilliporeSigma), 0.04% Pluronic F-127 (Thermo Fisher Scientific), and 4 µM Fluo 4-AM (Dojindo laboratories). Cells were then washed with HEPES-based buffer, seeded into 96-well black plates (1×10^4 cells/well), and stimulated with 0.5–1,000 nM LTB₄ or 2 µM Ionomycin (MilliporeSigma). Assay plates were then analyzed using FlexStation 3 (Molecular Devices).

TAXIScan chemotaxis assay. Chemotaxis of RAW264.7 cells toward 100 nM LTB₄ or ethanol (as a vehicle control) was monitored using TAXIScan-FL (Effector Cell Institute Frontier), as described previously (95). Phase-contrast sequential images were acquired at 1-minute intervals for 45 minutes and stacked using ImageJ. Chemotactic parameters (velocity and directionality) were analyzed with the ImageJ Manual Tracking plug-in and the ImageJ Chemotaxis and Migration tools plug-in.

ELISA. For VEGF-A protein expression analysis, culture media were collected in M2 BMDMs from BLT1-WT or BLT1-KO mice after stimulation with 500 nM LTB₄ or ethanol (as a vehicle control) for 4 hours. VEGF-A was measured culture media using the Mouse VEGF Quantikine ELISA Kit (R&D Systems) according to the manufacturer's instructions.

Statistics. Data are expressed as the mean ± SEM of at least 3 independent mice or eyes. Two data sets were compared using 2-tailed Student's *t* test. Multiple comparisons were performed using 1-way ANOVA followed by Bonferroni's, Newman-Keuls, or Dunnett's post hoc test, and 2-way ANOVA followed by Bonferroni's post hoc test. *P* value of less than 0.05 was considered statistically significant. All statistical analyses were performed using Prism version 5.0 (GraphPad Software).

Study approval. All animal studies and procedures were approved by the Ethics Committees on Animal Experimentation in Juntendo University (approval nos. 250224, 260166, 270161, 280167, and 290171). All the studies in this manuscript were carried out in accordance with approved guidelines and regulations.

Author contributions

FS and TY designed all experiments. FS, MO, KI, HA, and MRK performed the experiments. TK, MO, KS, TO, KI, TN, SN, SY, TI, HA, MRK, AHM, JMP, KHS, and TY helped acquire and analyze data. TY performed experiments. FS, AHM, and TY wrote the manuscript.

Acknowledgments

This work was supported by Grants-in-Aid for Scientific Research (KAKENHI) from the Ministry of Education, Culture, Sports, Science, and Technology (MEXT) of the Japan Society for the Promotion of Science (JSPS) (grant nos. 22116001, 22116002, 15H05897, 15H05904, 15H04708, and 18H02627 to TY; 25860223, 15K19032, and 17K08664 to TK; 24590386, 15K08316, and 18K06923 to KS; and 25460374, 16K08596, and 15KK0320 to TO) and by grants from the Naito Foundation, the Ono Medical Research Foundation, the Uehara Memorial Foundation, the Mitsubishi Foundation, and the Takeda Science Foundation. This study was supported in part by a Grant-in-Aid (S1311011 to TY) from the Foundation for Strategic Research Projects in Private Universities of the MEXT and by a grant from the Institute for Environmental and Gender-Specific

Medicine. We thank the Research Center for Human Disease Modeling (Kyushu University), the Research Support Center of the Division of Molecular and Biochemical Research (Juntendo University), and the Imaging Core Laboratory of the Institute of Medical Science (The University of Tokyo) for technical support. We also thank Eiichi Hasegawa (Harvard Medical School, Boston, Massachusetts, USA) and Akihiko Yoshimura (Keio University, Tokyo, Japan) for technical support of AMD model and BM transplantation, Takako Ichiki (California Institute of Technology, Pasadena, California, USA) for technical support of chemotaxis assay, and Miki Honda (Juntendo University), Akira Matsuda (Juntendo University), and the members of our laboratory for advice and helpful discussion.

Address correspondence to: Takehiko Yokomizo, Department of Biochemistry, Juntendo University School of Medicine, Hongo 2-1-1, Bunkyo-ku, Tokyo 113-8421, Japan. Phone: 81.3.5802.1030; Email: yokomizo-tky@umin.ac.jp.

TK's present address is: Department of Medical Cell Biology, Institute of Molecular Embryology and Genetics, Kumamoto University, Kumamoto, Japan.

FS's present address is: Department of Cell Signaling, Graduate School of Medical and Dental Sciences, Tokyo Medical and Dental University, Tokyo, Japan.

-
1. Global data on visual impairment 2010. World Health Organization. <http://www.who.int/blindness/publications/globaldata/en/>. Accessed August 20, 2018.
 2. Ambati J, Atkinson JP, Gelfand BD. Immunology of age-related macular degeneration. *Nat Rev Immunol*. 2013;13(6):438–451.
 3. Carr AJ, Smart MJ, Ramsden CM, Powner MB, da Cruz L, Coffey PJ. Development of human embryonic stem cell therapies for age-related macular degeneration. *Trends Neurosci*. 2013;36(7):385–395.
 4. Fritsche LG, Fariss RN, Stambolian D, Abecasis GR, Curcio CA, Swaroop A. Age-related macular degeneration: genetics and biology coming together. *Annu Rev Genomics Hum Genet*. 2014;15:151–171.
 5. Falavarjani KG, Nguyen QD. Adverse events and complications associated with intravitreal injection of anti-VEGF agents: a review of literature. *Eye (Lond)*. 2013;27(7):787–794.
 6. Yokomizo T, Izumi T, Chang K, Takuwa Y, Shimizu T. A G-protein-coupled receptor for leukotriene B4 that mediates chemotaxis. *Nature*. 1997;387(6633):620–624.
 7. Afonso PV, et al. LTB4 is a signal-relay molecule during neutrophil chemotaxis. *Dev Cell*. 2012;22(5):1079–1091.
 8. Lämmermann T, et al. Neutrophil swarms require LTB4 and integrins at sites of cell death in vivo. *Nature*. 2013;498(7454):371–375.
 9. Nakamura M, Shimizu T. Leukotriene receptors. *Chem Rev*. 2011;111(10):6231–6298.
 10. Yokomizo T. Two distinct leukotriene B4 receptors, BLT1 and BLT2. *J Biochem*. 2015;157(2):65–71.
 11. Tager AM, Dufour JH, Goodarzi K, Mercury SD, von Andrian UH, Luster AD. BLTR mediates leukotriene B(4)-induced chemotaxis and adhesion and plays a dominant role in eosinophil accumulation in a murine model of peritonitis. *J Exp Med*. 2000;192(3):439–446.
 12. Tager AM, et al. Leukotriene B4 receptor BLT1 mediates early effector T cell recruitment. *Nat Immunol*. 2003;4(10):982–990.
 13. Terawaki K, et al. Absence of leukotriene B4 receptor 1 confers resistance to airway hyperresponsiveness and Th2-type immune responses. *J Immunol*. 2005;175(7):4217–4225.
 14. Toda A, Terawaki K, Yamazaki S, Saeki K, Shimizu T, Yokomizo T. Attenuated Th1 induction by dendritic cells from mice deficient in the leukotriene B4 receptor 1. *Biochimie*. 2010;92(6):682–691.
 15. Kim ND, Chou RC, Seung E, Tager AM, Luster AD. A unique requirement for the leukotriene B4 receptor BLT1 for neutrophil recruitment in inflammatory arthritis. *J Exp Med*. 2006;203(4):829–835.
 16. Subbarao K, et al. Role of leukotriene B4 receptors in the development of atherosclerosis: potential mechanisms. *Arterioscler Thromb Vasc Biol*. 2004;24(2):369–375.
 17. Bäck M, Bu DX, Bränström R, Sheikine Y, Yan ZQ, Hansson GK. Leukotriene B4 signaling through NF-kappaB-dependent BLT1 receptors on vascular smooth muscle cells in atherosclerosis and intimal hyperplasia. *Proc Natl Acad Sci USA*. 2005;102(48):17501–17506.
 18. Kihara Y, et al. The leukotriene B4 receptor, BLT1, is required for the induction of experimental autoimmune encephalomyelitis. *Biochem Biophys Res Commun*. 2010;394(3):673–678.
 19. Sumida H, et al. Interplay between CXCR2 and BLT1 facilitates neutrophil infiltration and resultant keratinocyte activation in a murine model of imiquimod-induced psoriasis. *J Immunol*. 2014;192(9):4361–4369.
 20. Li P, et al. LTB4 promotes insulin resistance in obese mice by acting on macrophages, hepatocytes and myocytes. *Nat Med*. 2015;21(3):239–247.
 21. Pelegrin P, Surprenant A. Dynamics of macrophage polarization reveal new mechanism to inhibit IL-1beta release through pyrophosphates. *EMBO J*. 2009;28(14):2114–2127.
 22. Sindrilaru A, et al. An unrestrained proinflammatory M1 macrophage population induced by iron impairs wound healing in humans and mice. *J Clin Invest*. 2011;121(3):985–997.
 23. Xu H, et al. Notch-RBP-J signaling regulates the transcription factor IRF8 to promote inflammatory macrophage polarization. *Nat Immunol*. 2012;13(7):642–650.

24. Klug F, et al. Low-dose irradiation programs macrophage differentiation to an iNOS⁺/M1 phenotype that orchestrates effective T cell immunotherapy. *Cancer Cell*. 2013;24(5):589–602.
25. Lu G, et al. Myeloid cell-derived inducible nitric oxide synthase suppresses M1 macrophage polarization. *Nat Commun*. 2015;6:6676.
26. Verreck FA, et al. Human IL-23-producing type 1 macrophages promote but IL-10-producing type 2 macrophages subvert immunity to (myco)bacteria. *Proc Natl Acad Sci USA*. 2004;101(13):4560–4565.
27. Iwata Y, et al. Aberrant macrophages mediate defective kidney repair that triggers nephritis in lupus-susceptible mice. *J Immunol*. 2012;188(9):4568–4580.
28. Bayer C, et al. Human cytomegalovirus infection of M1 and M2 macrophages triggers inflammation and autologous T-cell proliferation. *J Virol*. 2013;87(1):67–79.
29. Deng T, et al. Class II major histocompatibility complex plays an essential role in obesity-induced adipose inflammation. *Cell Metab*. 2013;17(3):411–422.
30. Cucak H, Grunnet LG, Rosendahl A. Accumulation of M1-like macrophages in type 2 diabetic islets is followed by a systemic shift in macrophage polarization. *J Leukoc Biol*. 2014;95(1):149–160.
31. Biswas SK, Mantovani A. Macrophage plasticity and interaction with lymphocyte subsets: cancer as a paradigm. *Nat Immunol*. 2010;11(10):889–896.
32. Satoh T, et al. The Jmjd3-Irf4 axis regulates M2 macrophage polarization and host responses against helminth infection. *Nat Immunol*. 2010;11(10):936–944.
33. Egawa M, et al. Inflammatory monocytes recruited to allergic skin acquire an anti-inflammatory M2 phenotype via basophil-derived interleukin-4. *Immunity*. 2013;38(3):570–580.
34. Odegaard JI, et al. Macrophage-specific PPAR γ controls alternative activation and improves insulin resistance. *Nature*. 2007;447(7148):1116–1120.
35. Satoh T, et al. Critical role of Trib1 in differentiation of tissue-resident M2-like macrophages. *Nature*. 2013;495(7442):524–528.
36. Colegio OR, et al. Functional polarization of tumour-associated macrophages by tumour-derived lactic acid. *Nature*. 2014;513(7519):559–563.
37. Shaul ME, Bennett G, Strissel KJ, Greenberg AS, Obin MS. Dynamic, M2-like remodeling phenotypes of CD11c⁺ adipose tissue macrophages during high-fat diet-induced obesity in mice. *Diabetes*. 2010;59(5):1171–1181.
38. Marchetti V, et al. Differential macrophage polarization promotes tissue remodeling and repair in a model of ischemic retinopathy. *Sci Rep*. 2011;1:76.
39. Shechter R, et al. Recruitment of beneficial M2 macrophages to injured spinal cord is orchestrated by remote brain choroid plexus. *Immunity*. 2013;38(3):555–569.
40. Huber S, Hoffmann R, Muskens F, Voehringer D. Alternatively activated macrophages inhibit T-cell proliferation by Stat6-dependent expression of PD-L2. *Blood*. 2010;116(17):3311–3320.
41. Spite M, et al. Deficiency of the leukotriene B4 receptor, BLT-1, protects against systemic insulin resistance in diet-induced obesity. *J Immunol*. 2011;187(4):1942–1949.
42. Parsa R, et al. Adoptive transfer of immunomodulatory M2 macrophages prevents type 1 diabetes in NOD mice. *Diabetes*. 2012;61(11):2881–2892.
43. Huang SC, et al. Cell-intrinsic lysosomal lipolysis is essential for alternative activation of macrophages. *Nat Immunol*. 2014;15(9):846–855.
44. Shiraishi M, et al. Alternatively activated macrophages determine repair of the infarcted adult murine heart. *J Clin Invest*. 2016;126(6):2151–2166.
45. Liao X, et al. Krüppel-like factor 4 regulates macrophage polarization. *J Clin Invest*. 2011;121(7):2736–2749.
46. Arranz A, et al. Akt1 and Akt2 protein kinases differentially contribute to macrophage polarization. *Proc Natl Acad Sci USA*. 2012;109(24):9517–9522.
47. Han MS, et al. JNK expression by macrophages promotes obesity-induced insulin resistance and inflammation. *Science*. 2013;339(6116):218–222.
48. Neves J, et al. Immune modulation by MANF promotes tissue repair and regenerative success in the retina. *Science*. 2016;353(6294):aaf3646.
49. Nakao S, et al. VAP-1-mediated M2 macrophage infiltration underlies IL-1 β - but not VEGF-A-induced lymph- and angiogenesis. *Am J Pathol*. 2011;178(4):1913–1921.
50. Horie S, et al. CD200R signaling inhibits pro-angiogenic gene expression by macrophages and suppresses choroidal neovascularization. *Sci Rep*. 2013;3:3072.
51. Sene A, et al. Impaired cholesterol efflux in senescent macrophages promotes age-related macular degeneration. *Cell Metab*. 2013;17(4):549–561.
52. Nakamura R, et al. IL10-driven STAT3 signalling in senescent macrophages promotes pathological eye angiogenesis. *Nat Commun*. 2015;6:7847.
53. Zandi S, et al. ROCK-isoform-specific polarization of macrophages associated with age-related macular degeneration. *Cell Rep*. 2015;10(7):1173–1186.
54. Lv J, Xiong Y, Li W, Yang W, Zhao L, He R. BLT1 Mediates Bleomycin-Induced Lung Fibrosis Independently of Neutrophils and CD4⁺ T Cells. *J Immunol*. 2017;198(4):1673–1684.
55. Ying W, et al. Adipose tissue B2 cells promote insulin resistance through leukotriene LTB4/LTB4R1 signaling. *J Clin Invest*. 2017;127(3):1019–1030.
56. Bodduluri SR, et al. Mast Cell-Dependent CD8(+) T-cell Recruitment Mediates Immune Surveillance of Intestinal Tumors in Apc(Min/+) Mice. *Cancer Immunol Res*. 2018;6(3):332–347.
57. Lambert V, et al. Laser-induced choroidal neovascularization model to study age-related macular degeneration in mice. *Nat Protoc*. 2013;8(11):2197–2211.
58. Ferrara N, Mass RD, Campa C, Kim R. Targeting VEGF-A to treat cancer and age-related macular degeneration. *Annu Rev Med*. 2007;58:491–504.

59. Ishikawa K, Kannan R, Hinton DR. Molecular mechanisms of subretinal fibrosis in age-related macular degeneration. *Exp Eye Res.* 2016;142:19–25.
60. Ambati J, et al. An animal model of age-related macular degeneration in senescent Ccl-2- or Ccr-2-deficient mice. *Nat Med.* 2003;9(11):1390–1397.
61. Takeda A, et al. CCR3 is a target for age-related macular degeneration diagnosis and therapy. *Nature.* 2009;460(7252):225–230.
62. Yokomizo T, Kato K, Terawaki K, Izumi T, Shimizu T. A second leukotriene B(4) receptor, BLT2. A new therapeutic target in inflammation and immunological disorders. *J Exp Med.* 2000;192(3):421–432.
63. Okuno T, Iizuka Y, Okazaki H, Yokomizo T, Taguchi R, Shimizu T. 12(S)-Hydroxyheptadeca-5Z, 8E, 10E-trienoic acid is a natural ligand for leukotriene B4 receptor 2. *J Exp Med.* 2008;205(4):759–766.
64. Iizuka Y, et al. Protective role of the leukotriene B4 receptor BLT2 in murine inflammatory colitis. *FASEB J.* 2010;24(12):4678–4690.
65. Liu M, et al. 12-Hydroxyheptadecatrienoic acid promotes epidermal wound healing by accelerating keratinocyte migration via the BLT2 receptor. *J Exp Med.* 2014;211(6):1063–1078.
66. Shigematsu M, et al. Leukotriene B4 receptor type 2 protects against pneumolysin-dependent acute lung injury. *Sci Rep.* 2016;6:34560.
67. Talahalli R, Zarini S, Sheibani N, Murphy RC, Gubitosi-Klug RA. Increased synthesis of leukotrienes in the mouse model of diabetic retinopathy. *Invest Ophthalmol Vis Sci.* 2010;51(3):1699–1708.
68. Subramanian P, Mendez EF, Becerra SP. A Novel Inhibitor of 5-Lipoxygenase (5-LOX) Prevents Oxidative Stress-Induced Cell Death of Retinal Pigment Epithelium (RPE) Cells. *Invest Ophthalmol Vis Sci.* 2016;57(11):4581–4588.
69. Espinosa-Heidmann DG, Caicedo A, Hernandez EP, Csaky KG, Cousins SW. Bone marrow-derived progenitor cells contribute to experimental choroidal neovascularization. *Invest Ophthalmol Vis Sci.* 2003;44(11):4914–4919.
70. Kezic JM, McMenamin PG. The effects of CX3CR1 deficiency and irradiation on the homing of monocyte-derived cell populations in the mouse eye. *PLoS ONE.* 2013;8(7):e68570.
71. Espinosa-Heidmann DG, et al. Bone marrow transplantation transfers age-related susceptibility to neovascular remodeling in murine laser-induced choroidal neovascularization. *Invest Ophthalmol Vis Sci.* 2013;54(12):7439–7449.
72. Singh V, Jaini R, Torricelli AA, Tuohy VK, Wilson SE. A method to generate enhanced GFP+ chimeric mice to study the role of bone marrow-derived cells in the eye. *Exp Eye Res.* 2013;116:366–370.
73. O'Koren EG, Mathew R, Saban DR. Fate mapping reveals that microglia and recruited monocyte-derived macrophages are definitively distinguishable by phenotype in the retina. *Sci Rep.* 2016;6:20636.
74. Sakurai E, Anand A, Ambati BK, van Rooijen N, Ambati J. Macrophage depletion inhibits experimental choroidal neovascularization. *Invest Ophthalmol Vis Sci.* 2003;44(8):3578–3585.
75. Zhou W, et al. Periostin secreted by glioblastoma stem cells recruits M2 tumour-associated macrophages and promotes malignant growth. *Nat Cell Biol.* 2015;17(2):170–182.
76. Kuniyeda K, Okuno T, Terawaki K, Miyano M, Yokomizo T, Shimizu T. Identification of the intracellular region of the leukotriene B4 receptor type 1 that is specifically involved in Gi activation. *J Biol Chem.* 2007;282(6):3998–4006.
77. Bacci M, et al. Macrophages are alternatively activated in patients with endometriosis and required for growth and vascularization of lesions in a mouse model of disease. *Am J Pathol.* 2009;175(2):547–556.
78. Hughes R, et al. Perivascular M2 Macrophages Stimulate Tumor Relapse after Chemotherapy. *Cancer Res.* 2015;75(17):3479–3491.
79. Zhou Y, et al. M2 Macrophages Enhance Pathological Neovascularization in the Mouse Model of Oxygen-Induced Retinopathy. *Invest Ophthalmol Vis Sci.* 2015;56(8):4767–4777.
80. Griffiths RJ, et al. Leukotriene B4 plays a critical role in the progression of collagen-induced arthritis. *Proc Natl Acad Sci USA.* 1995;92(2):517–521.
81. Mathis SP, Jala VR, Lee DM, Haribabu B. Nonredundant roles for leukotriene B4 receptors BLT1 and BLT2 in inflammatory arthritis. *J Immunol.* 2010;185(5):3049–3056.
82. Okamoto F, Saeki K, Sumimoto H, Yamasaki S, Yokomizo T. Leukotriene B4 augments and restores Fc gammaRs-dependent phagocytosis in macrophages. *J Biol Chem.* 2010;285(52):41113–41121.
83. Funk CD. Leukotriene modifiers as potential therapeutics for cardiovascular disease. *Nat Rev Drug Discov.* 2005;4(8):664–672.
84. Wickström M, Larsson R, Nygren P, Gullbo J. Aminopeptidase N (CD13) as a target for cancer chemotherapy. *Cancer Sci.* 2011;102(3):501–508.
85. Saeki K, Yokomizo T. Identification, signaling, and functions of LTB4 receptors. *Semin Immunol.* 2017;33:30–36.
86. Iwamoto S, et al. Non-steroidal anti-inflammatory drug delays corneal wound healing by reducing production of 12-hydroxyheptadecatrienoic acid, a ligand for leukotriene B4 receptor 2. *Sci Rep.* 2017;7(1):13267.
87. CATT Research Group, et al. Ranibizumab and bevacizumab for neovascular age-related macular degeneration. *N Engl J Med.* 2011;364(20):1897–1908.
88. Syed BA, Evans JB, Bielory L. Wet AMD market. *Nat Rev Drug Discov.* 2012;11(11):827.
89. Gao S, et al. PEDF mediates pathological neovascularization by regulating macrophage recruitment and polarization in the mouse model of oxygen-induced retinopathy. *Sci Rep.* 2017;7:42846.
90. Nakama T, et al. Therapeutic Effect of Novel Single-Stranded RNAi Agent Targeting Periostin in Eyes with Retinal Neovascularization. *Mol Ther Nucleic Acids.* 2017;6:279–289.
91. Matsunobu T, Okuno T, Yokoyama C, Yokomizo T. Thromboxane A synthase-independent production of 12-hydroxyheptadecatrienoic acid, a BLT2 ligand. *J Lipid Res.* 2013;54(11):2979–2987.
92. Okuno T, et al. Altered eicosanoid production and phospholipid remodeling during cell culture. *J Lipid Res.* 2018;59(3):542–549.
93. Sasaki F, et al. Biochemical and immunological characterization of a novel monoclonal antibody against mouse leukotriene B4 receptor 1. *PLoS One.* 2017;12(9):e0185133.
94. Tsutsumi-Miyahara C, et al. The relative contributions of each subset of ocular infiltrated cells in experimental choroidal neovascularisation. *Br J Ophthalmol.* 2004;88(9):1217–1222.
95. Ichiki T, et al. Modulation of leukotriene B4 receptor 1 signaling by receptor for advanced glycation end products (RAGE). *FASEB J.* 2016;30(5):1811–1822.